HHS Public Access

Author manuscript

Med Phys. Author manuscript; available in PMC 2024 November 01.

Published in final edited form as:

Med Phys. 2023 November ; 50(11): 6779–6788. doi:10.1002/mp.16713.

Characterization of Single- and Multi-energy CT Performance of an Oral Dark Borosilicate Contrast Media using a Clinical Photon-Counting-Detector CT Platform

Liqiang Ren, Ph.D.[1,†], **Yuxin Sun, M.S.**[2], **Benjamin Yeh, M.D.**[2], **Jeffrey F. Marsh**[1], **Timothy N. Winfree**[1], **Kristin A. Burke**[1], **Kishore Rajendran, Ph.D.**[1], **Cynthia H. McCollough, Ph.D.**[1], **Achille Mileto, M.D.**[3], **Joel G. Fletcher, M.D.**[1], **Shuai Leng, Ph.D.**[1,*]

[1]Department of Radiology, Mayo Clinic, Rochester, MN, US

[2]NEXTRAST, INC., Hillsborough, CA, US

[3]Department of Radiology, Virginia Mason Medical Center, Seattle, WA, US

Abstract

Background: The feasibility of oral dark contrast media is under exploration in abdominal CT applications. One of the experimental contrast media in this class is dark borosilicate contrast media (DBCM), which has a CT attenuation lower than that of intra-abdominal fat.

Purpose: To evaluate the performances of DBCM using single- and multi-energy CT imaging on a clinical photon-counting-detector CT (PCD-CT).

Methods: Five vials, three with iodinated contrast agent (5, 10, and 15 mg/mL; Omnipaque 350) and two with DBCM (6 and 12%; Nextrast, Inc), and one solid-water rod (neutral contrast agent) were inserted into two multi-energy CT phantoms, and scanned on a clinical PCD-CT system (NAEOTOM Alpha) at 90, 120, 140, Sn100, and Sn140 kV (Sn: tin filter) in multi-energy mode. CARE keV IQ level was 180 (CTDIvol: 3.0 and 12.0 mGy for the small and large phantoms, respectively). Low-energy threshold images were reconstructed with a quantitative kernel (Qr40, iterative reconstruction strength 2) and slice thickness/increment of 2.0/2.0 mm. Virtual monoenergetic images (VMIs) were reconstructed from 40 to 140 keV at 10 keV increments. On all images, average CT numbers for each vial/rod were measured using circular region-of-interests and averaged over eight slices. The contrast-to-noise ratio (CNR) of iodine (5 mg/mL) against DBCM was calculated and plotted against tube potential and VMI energy level, and compared to the CNR of iodine against water. Similar analyses were performed on iodine maps and VNC images derived from the multi-energy scan at 120 kV.

Results: With increasing kV or VMI keV, the negative HU of DBCM decreased only slightly, whereas the positive HU of iodine decreased across all contrast concentrations and phantom sizes. CT numbers for DBCM decreased from −178.5±9.6 to −194.4±6.3 HU (small phantom) and from −181.7±15.7 to −192.1±11.9 HU (large phantom) for DBCM-12% from 90 to Sn140 kV; on VMIs, the CT numbers for DBCM decreased minimally from −147.1±15.7 to −185.1±9.2

[*]**Corresponding Author:** Shuai Leng, Ph.D., Department of Radiology, Mayo Clinic, 200 1st Street SW, Rochester, MN 55905, Phone: (507) 293-4233, Leng.Shuai@mayo.edu.

[†]Current: Department of Radiology, UT Southwestern Medical Center, Dallas, TX, US

HU (small phantom) and −158.8±28.6 to −188.9±14.7 HU (large phantom) from 40 to 70 keV, but remained stable from 80 to 140 keV. The highest iodine CNR against DBCM in low-energy threshold images was seen at 90 or Sn140 kV for the small phantom, whereas all CNR values from low-energy threshold images for the large phantom were comparable. The CNR values of iodine against DBCM computed on VMIs were highest at 40 or 70 keV depending on iodine and DBCM concentrations. The CNR values of iodine against DBCM were consistently higher than iodine to water (up to 460% higher dependent on energy level). Further, the CNR of iodine compared to DBCM is less affected by VMI energy level than the identical comparison between iodine and water: CNR values at 140 keV were reduced by 46.6% (small phantom) or 42.6% (large phantom) compared to 40 keV; CNR values for iodine compared to water were reduced by 86.3% and 83.8% for similar phantom sizes, respectively. Compared to 70 keV VMI, the iodine CNR against DBCM was 13–79% lower on iodine maps and VNC.

Conclusions: When evaluated at different tube potentials and VMI energy levels using a clinical PCD-CT system, DBCM showed consistently higher CNR compared to iodine versus water (a neutral contrast).

Keywords

Dark Borosilicate Contrast Media (DBCM); photon-counting-detector CT (PCD-CT); contrast-to-noise ratio (CNR); multi-energy spectral post processing; virtual monoenergetic images (VMIs)

1. Introduction

In many clinical tasks involving bowel or peritoneal diseases, positive or neutral enteric contrast media are commonly administered to patients prior to their computed tomography (CT) scan to improve the visualization of small bowel inflammation, edema, or mass (whether intraluminal, mural, or serosal).[1] The administration of positive enteric contrast media may be problematic in certain clinical scenarios where intravenous iodinated contrast is also used, as it can be challenging to differentiate between positive oral contrast within the gut lumen and iodine-enhanced small bowel wall or mass due to similar CT numbers.[2,3] Neutral oral contrast media, including water or flavored beverages, which often contain sorbitol, mannitol, and xantham gum, which are added to improve distension the small bowel lumen, and are routinely used in CT enterography to maximize the conspicuity of small bowel-related pathologies. While this approach improves radiologist performance for detection of mural masses and inflammation,[4–6] it may result in suboptimal image contrast between the bowel wall and small intraluminal or serosal masses (such as polyps or peritoneal disease).[7,8]

Oral dark contrast media have recently been developed and their feasibility for clinical abdominal CT applications has been tested in preliminary studies.[9–11] For example, a stable, drinkable foam was orally administered to twenty-five consented volunteers and the intraluminal CT numbers were demonstrated to be around –550 HU, which appeared promisingly to be a great bowel lumen-to-wall contrast.[9] In another study, a diluted emulsion of arachis oil (Calogen®, a fat density food supplement) was assessed in upper abdominal CT exams and demonstrated a significant improvement in distension and anatomical visualization of the stomach and proximal duodenum.[10]

Dark borosilicate contrast media (DBCM, Nextrast, Inc.), another type of oral dark contrast media, shows negative CT numbers that are lower than intra-abdominal fat and is FDA approved for clinical trials as an investigative new drug.[11] Such oral contrast media may possess diagnostic advantages compared to positive and neutral contrast media by increasing observed CT number differences between the bowel wall and the adjacent lumen or mesentery. In this phantom study we simulate the CT number and noise of the enhancing small bowel wall using a solution of iodine contrast, and the CT number and noise of the enteric contrast-filled gut lumen with DBCM and solid water.

Photon-counting-detector CT systems (PCD-CT) have recently been tested and has showed substantial benefits in various clinical areas compared to energy-integrating-based CT platforms.[12–14] However, to the best of our knowledge, the spectral performance of DBCM has not yet been evaluated on any of the preclinical or clinical PCD-CT systems.[15] This phantom study represents the first study to systematically evaluate the performance of DBCM including CT number, noise, and contrast-to-noise ratio (CNR) using single- and multi-energy CT imaging protocols on a clinical PCD-CT system.

2. Methods

2.1. Phantom Design

A multi-energy CT phantom (model 1472, Gammex™ Technology) was used for this study. The phantom consisted of two sections: a cylindrical phantom (diameter: 20 cm; depth: 16.5 cm) simulating a head or a patient with a small-size abdomen, and an external ring (lateral: 40 cm; anterior-posterior: 30 cm; depth: 16.5 cm) mimicking a patient with large body size when placed around the small phantom. A total of 16 drilled slots (10 for the small phantom, and 6 for the larger body ring) were available for the two sections of the phantom. Quantitative analysis can be performed by inserting solid rods or other materials of interest containing contrast agents, or mimicking various tissue types such as bone, adipose, and brain into those slots.

For the purpose of this study, a solid water rod (mimicking neutral contrast in bowel lumen) and vials containing various contrast media were inserted into the phantom slots. Forty-five contrast media vials were prepared and mixed well prior to CT scanning. Each slot contained three smaller contrast vials stacked and glued vertically to form a “vial rod” (Figure 1a). The vial rods were labeled and inserted into the phantom slots, as shown in Figure 1. The materials of interests in this study were iodinated contrast materials (Omnipaque 350, GE Healthcare) with mass concentration at 5, 10, and 15 mg/mL, and DBCM with a mass percentage of 6% and 12% (referred to as DBCM-6% and DBCM-12%), each contained in a separate vial. The iodine concentration of 5 mg/mL was chosen to simulate the CT number of normal-enhancing bowel, and iodine concentrations of 10 and 15 mg/mL were chosen to mimic inflamed hyperenhancing bowel or masses on clinical CT scans of the abdomen acquired after intravenous contrast administration. The DBCM mass concentrations were determined to result in CT attenuation of about −200 Hounsfield Units (HU) to −100 HU at 120 kV, which was close to a previously reported attenuation value (−150 HU).[11]

2.2. CT Data Acquisition and Reconstruction

Phantom scans were performed on a clinical PCD-CT system (NAEOTOM Alpha, Siemens Healthineers) using the multi-energy mode (144 × 0.4 mm collimation). Automatic exposure control (CARE keV and CAREDose 4D) was enabled with the IQ level set to 180, resulting in radiation output (CTDIvol) values of 3.0 and 12.0 mGy for the small and large phantoms, respectively. Five tube potentials (90, 120, 140, Sn100, and Sn140 kV) were manually selected. Low-energy threshold (T3D) images which used all detected photons but no spectral properties of the PCD were reconstructed for each kV, with a single energy threshold at 20 keV set by the manufacture to eliminate electronic noise below this energy level.[14] Series of virtual monoenergetic images (VMIs) were derived from each multi-energy scan at five different tube potentials with VMI energy levels ranging from 40 to 130 keV for 90 kV, 40 to 140 keV for 120 and 140 kV, and 60–140 keV for Sn100 and Sn140 kV (all in 10 keV increments). The available keV range of VMIs for each tube potential (kV) is pre-defined by the manufacturer. Additionally, iodine maps and virtual noncontrast (VNC) images were derived from the 120 kV multi-energy scan. All images were reconstructed using a quantitative kernel (Qr40) and iterative reconstruction at a strength level of 2 (QIR-2: Quantum Iterative Reconstruction; Siemens Healthcare GmBH). Note that QIR was enabled based on our clinical protocol to reflect the true noise magnitude and CNR values of DBCM imaging in potential patient applications. The slice thickness and increment were 2.0 and 2.0 mm for all of the reconstructed images. Detailed technical parameters for the clinical PCD-CT system can be found in the literature.[15] All scanning and reconstruction parameters are summarized in Table 1.

2.3. Data Processing and Analysis

The average CT numbers (in HU) were measured by drawing a circular region of interest (ROI) on each investigated material including three iodinated solutions, two DBCM-based suspensions, and one solid-water rod on low-energy threshold image, VMIs, iodine maps, and VNC images. The measurements were repeated and averaged over eight consecutive slices. The noise levels were derived as the standard deviation of all pixel values within the same ROIs used for averaged contrast measurements. An example of the ROI selections for three contrast materials (iodine at 5 and 15 mg/mL, DBCM at 12%) and water are indicated in Figure 2.

To gauge the relative conspicuity of enhancing bowel wall compared to enteric contrast media-filled gut lumen, a CNR reflecting the conspicuity of the gut wall compared to DBCM or solid water was calculated. To estimate the CNR of the gut wall against DBCM as an enteric contrast agent, the CNR of iodine (5 mg/mL) against DBCM (6% and 12%) were calculated and plotted against all tube potentials (kVs) on low-energy threshold images and all energy levels on VMIs. The iodine concentration of 5 mg/mL was selected to represent the maximal enhancement level of the bowel wall corresponding to 100–120 HU at 120 kV. On iodine maps and VNC images, all three iodine concentration levels were included for analysis. The CNR values of iodine against DBCM or solid water were calculated using Eqs. (1) and (2).

$$CNR_{I/DBCM} = \frac{CT\_Number(I) - CT\_Number(DBCM)}{\sqrt{\left(Noise_I^2 + Noise_{DBCM}^2\right)/2}} \quad (1)$$

$$CNR_{I/Water} = \frac{CT\_Number(I) - CT\_Number(Water)}{\sqrt{\left(Noise_I^2 + Noise_{Water}^2\right)/2}} \quad (2)$$

3. Results

3.1. Analysis on Low-energy Threshold Images and VMIs

3.1.1 Representative Images—Figure 3 shows representative low-energy threshold images of the small phantom acquired at five different kVs and the derived VMIs at 40, 50, 70, 100, and 140 keV (all derived from the 120 kV scan). Iodine (15 mg/mL), DBCM-12%, and solid-water were highlighted, and the window width/level was adjusted to 1000/200 HU for visual assessment. As anticipated, iodine signal is brighter at lower kV or VMI energy levels, while DBCM signal becomes slightly darker at first with the increase of the effective energy of data acquisition but gradually stabilizes afterwards, whereas the water signal remains around 0 HU across all energy levels. All low-energy threshold images and VMIs were carefully reviewed, and no obvious artifacts were observed except the VMIs derived from the Sn140 kV scan for the large phantom, which were excluded for further quantitative analysis.

3.1.2. CT Number and CNR Analysis (Small Phantom)—Figure 4 summarizes the attenuation properties of iodine, DBCM and water, and CNR calculations on all low-energy threshold images and VMIs acquired with the small phantom. As shown in Figure 4a (low-energy threshold images) and Figure 4d (VMIs), the positive iodine HU values increased with higher concentrations and decreased with increased effective energies of tube potentials or VMI keV levels, as expected. For example, the HU values decreased from 156.3±9.2 to 68.5±5.2 HU from 90 to Sn140 kV, and from 321.2±15.0 to 23.7±8.2 HU from 40 to 140 keV for the 5 mg/mL iodine solution.

The attenuation properties of DBCM at 6% and 12%, which has negative CT numbers, are demonstrated in Figure 4b (low-energy threshold images) and Figure 4e (VMIs). On low-energy threshold images, the CT numbers within DBCM slightly decreased from −97.8±10.0 to −105.1±9.4 HU for 6% DBCM, and −178.5±9.6 to −194.4±6.3 HU for 12% DBCM from 90 to Sn140 kV. The averaged noise levels were calculated as 10.2±0.9, 9.5±1.4, 9.2±1.4, 9.0±2.6, and 7.8±3.2 for 90, 120, 140, Sn100, and Sn140 kV, respectively.

On VMIs, the change of the negative HU values of DBCM depended on the concentration level and synthesized energy. For 6% DBCM, the negative HU values were slightly decreased from −87.7±14.5 to −101.0±9.2 HU in the energy range of 40 to 70 keV and remained stable from −102.3±9.3 to −105.2±9.2 HU at 80 to 140 keV. For 12% DBCM, the dependency on VMI keV levels was stronger than the 6% DBCM, with CT number

changing from −147.1±15.7 to −198.4±9.1 HU from 40 to 140 keV. As a reference, the HU values measured on the solid-water rod were stable in the range of [−5.4±8.7, 1.1±8.2 HU].

As indicated in Figure 4c (low-energy threshold images), the maximal CNR is seen at 90 kV for iodine against DBCM-6% (CNR: 26.5) and Sn140 kV for iodine against DBCM-12% (CNR: 45.5). From Figure 4f (VMIs), the CNR values computed on VMIs were highest at 40 keV for iodine against DBCM-6% (CNR: 27.8), and 70 keV for iodine against DBCM-12% (CNR: 32.4). As demonstrated in Figure 4c and 4f, the CNR values of iodine against DBCM were consistently higher than that of iodine against water, with an increase of 44–460% across the kV and VMI energy levels. Further in Figure 4f, the CNR of iodine against DBCM was less affected by energy levels: compared to 40 keV, CNR values at 140 keV were reduced by 46.6% for iodine against DBCM-6% and 86.3% for iodine against water.

Note that all VMIs used for CT number measurements and CNR analysis on the small phantom were derived from the 120 kV multi-energy scan. The results acquired with VMIs derived at other kV levels including 90, 140, Sn100, and Sn140 kV were summarized and plotted in Figure S1.

3.1.3. CT Number and CNR Analysis (Large Phantom)—The attenuation properties of iodine, DBCM, and water, and CNR calculations on all low-energy threshold images and VMIs are summarized in Figure 5 for the large phantom. The trend of positive iodine attenuations was similar to that on the small phantom and decreased with increased effective energies of tube potentials (Figure 5a) or VMI keV levels (Figure 5d). The negative HU values measured for DBCM attenuations are demonstrated in Figure 5b (low-energy threshold images) and Figure 5e (VMIs). On low-energy threshold images, there is a decrease in attenuation from −101.1±13.0 to −105.0±10.9 HU for DBCM-6%, and −181.7±15.7 to −192.1±11.9 HU for DBCM-12% from 90 to Sn140 kV. The averaged noise levels were calculated as 15.0±1.1, 14.8±1.2, 14.4±0.8, 12.1±1.7, and 12.1±2.0 for 90, 120, 140, Sn100, and Sn140 kVp, respectively.

On VMIs, the change in the negative HU values of DBCM depended on the concentration level and synthesized energy. For DBCM-6%, the negative HU values were slightly decreased from −95.8±25.7 to −101.4±13.3 HU in the energy range of 40 to 70 keV and remained stable from −102.8±12.6 to −104.5±12.0 HU at 80 to 140 keV. For DBCM-12%, the dependency on VMI keV levels was stronger than DBCM-6%, with −158.5±28.6 to −199.3±14.5 HU from 40 to 140 keV. As a reference, the HU values measured on the water rod were stable in the range of [−5.6±13.1, 8.0±21.7 HU].

As indicated in Figure 5c (low-energy threshold images) and Figure 5f (VMIs), all CNRs from the low-energy threshold images were comparable for iodine against DBCM-6% (minimum and maximum CNR: 14.4 at 140 or Sn140 kV and 16.9 at 90 kV), and iodine against DBCM-12% (minimum and maximum CNR: 19.6 at 140 kV and 21.6 at Sn100 kV). The CNR values computed on VMIs were highest at 40 keV for 6% DBCM (CNR: 16.2), and 70 keV for 12% DBCM (CNR: 20.3). As indicated in Figure 5f, the CNR values of iodine against DBCM were consistently higher than that of iodine against water, with an

increase of 50–460% across the energy level. Further in Figure 5f, the CNR of iodine against DBCM was less affected by energy levels: compared to 40 keV, CNR values at 140 keV were reduced by 42.6% for iodine against DBCM-6% and 83.8% for iodine against water.

Note that all VMIs used for CT number measurements and CNR analysis on the large phantom were derived from the 120 kV multi-energy scan. The results acquired with VMIs derived at other kV levels including 90, 140, and Sn100 (note: VMIs derived from Sn140 kV were excluded for quantitative analysis due to imaging artifacts) were summarized and plotted in Figure S2.

3.2. Analysis on Iodine Maps and VNC Images

Figure 6 shows VMI (70keV), iodine maps and VNC images derived from the multi-energy scan at 120 kV for three iodine samples (5, 10, and 15 mg/mL), DBCM-6%, DBCM-12%, and solid-water (window width/level: 400/40 HU). Note that the displayed values on the iodine maps were converted from concentration (mg/mL) to CT numbers (HU) at about 70 keV for convenience of comparing across different image types (e.g., VMI, iodine map, and VNC) using same metric. As anticipated, iodine signals were well maintained on the iodine maps compared to the 70 keV VMI, but completely eliminated from the VNC images. The DBCM signals were slightly positive on the iodine maps, which offset the HU values on VNC images to be even more negative than that of 70 keV VMI. The water signal remained around 0 HU across all spectral image types. Detailed CT number measurements are summarized in Table 2. All iodine maps and VNC images were carefully reviewed, and no obvious artifacts were observed.

CNR values for iodine at three different concentration levels each against water, DBCM-6%, or DBCM-12% were compared across three spectral reconstruction types (70 keV VMI, iodine map, and VNC) (Figure 7). All CNRs on 70 keV VMI were increased with higher iodine concentrations and DBCM concentrations. On the iodine map, the CNR values were also increased with higher iodine concentrations but remained comparable or even slightly lower with DBCM instead of water due to the positive HU values of DBCM on iodine maps. CNR values on VNC images were consistently lower than those calculated on the VMIs regardless of the phantom sizes.

4. Discussion

In this phantom study, the single- and multi-energy imaging performance of the DBCM was evaluated using a clinical PCD-CT platform. Low-energy threshold images acquired at five different kV levels (90, 120, 140, Sn100, and Sn140 kV), VMIs at energy levels (from 40 to 140 keV), iodine map, and VNC images were analyzed. Attenuation properties for iodinated contrast solutions (5, 10, and 15 mg/mL), DBCM (6 and 12%), and water (neutral contrast) were calculated for two phantoms sizes. CNR values of DBCM or water against iodine were derived to quantify the improvement in delineation between an iodine-enhanced bowel wall and a gut lumen filled with water or DBCM as ingested enteric contrast. The CNR values of iodine against DBCM were consistently higher than iodine against water (by up to 460%), with smaller CT number differences across different VMI energy levels: compared to 40 keV, CNR values at 140 keV were reduced by 46.6% (small phantom) or

42.6% (large phantom) for iodine against DBCM versus 86.3% and 83.8% for iodine against water, respectively.

The calculation of CNR reflects both attenuation property differences between positive iodine and negative DBCM (or neutral water), and noise performance. On low-energy threshold images, the maximal CNR of iodine against DBCM derived from low-energy threshold images was observed at either 90 kV or Sn140 kV for the small phantom due to the highest achievable iodine CT number or the lowest image noise level depending on the DBCM concentration levels. The benefits of using low tube voltage to boost the iodine contrast or additional filtration such as Tin materials to achieve improved noise performance have been reported in previous studies.[16] However, the reported studies using Tin filtration focused on non-contrast exams and a relatively low tube voltage such as 100 kV. As shown in our study, with high concentration of DBCM, the significant noise reduction of Sn140 kVp can offset the simultaneous reduction in iodine image contrast. For the large phantom, similar results were obtained but with comparable CNR values across all kVp levels.

On the VMIs, the maximal CNR values were seen at either 40 keV, where the attenuation was highest for iodine, or 70 keV, where the noise was optimized, depending on relative iodine and DBCM concentration levels. Additionally, the CNR values for iodine against DBCM could be segmented into two sections corresponding to the energy ranges of 40–70 keV and 80–140 keV, where the CNR at 40–70 keV was in general higher than the other section. This trend was not observed for CNR values calculated between iodine and water, however. This observation occurred because water is very stable in CT number at about 0 HU across all the energy levels, while DBCM CT number changes as the VMI energy level changes from 40–70 keV. The optimal VMI energy level of 70 keV when imaging iodine and DBCM is of clinical significance as both overall optimal image quality and the highest CNR are maintained. In iodine and water imaging, the VMI energy level of 40 keV would provide the highest CNR, but the VMIs at 40 keV typically have artifacts and unnatural texture and are not preferred in clinical use. Therefore, an energy level between 40 and 70 keV, such as 50 keV, has been recommended as compromise between the highest CNR and optimal image quality.[17–20] Simultaneous evaluations of multiple VMI data could be possible yet results in longer reporting times. Given our results, however, reconstruction of VMIs with multiple energy levels would likely result in little diagnostic benefit given the high CNR of iodine compared to DBCM at approximately 70 keV.

The attenuation properties and CNR were also analyzed on iodine maps and VNC images derived from the multi-energy scan at 120 kV. Compared to the low-energy threshold images or VMIs, no improvements were noticed on the iodine maps and VNC images. This is because replacing neutral contrast agents such as water with dark oral contrast agents such as DBCM could complicate the material decomposition process due to different basis materials. With DBCM and associated high CNR of iodine against DBCM, however, there would be little ambiguity in delineating bowel wall from bowel lumen on either low-energy thresholds images and/or VMIs, which in turn reduces the need to use material decomposition images to resolve ambiguous densities.

Imaging of iodine and DBCM with PCD-CT is expected to provide the following clinical benefits compared to using conventional CT platforms based on energy-integrating-detectors for small bowel imaging. First, the CNR of iodine against DBCM can be increased due to equal photon weighting in PCD-CT, particularly on low-energy threshold images. Second, the overall imaging quality and noise are lower due to the elimination of electronic noise by setting a low energy threshold at 20 keV, or they can be maintained with reduced radiation dose. Third, thanks to the reduced noise, the ability of using thin slices is increased to effectively decrease partial volume effects. Last, both low-energy threshold images and VMIs can be obtained from the same scan due to the intrinsic spectral sensitivity of PCD-CT, thus improving the clinical workflow.

Our study had two limitations. First, only two phantom sizes were used to cover a reasonable range of patient habitus. Since some evaluations seemed highly dependent on phantom size such as the CNR values on low-energy threshold images, another phantom between 20 cm and 40 cm, and one corresponding to obese patients, would be beneficial to fully understand the spectral imaging performance of DBCM. Second, DBCM remains experimental and is not FDA approved for clinical use and the safety profile of DBCM has not been released. Therefore, the concentrations of DBCM, 6% and 12% were selected based on manufacturer recommendations to achieve a negative enhancement of −200 to −100 HU in small bowel lumen. The dose and mass concentration of the DBCM and its complete safety profile warrant future clinical studies.

5. Conclusion

The spectral imaging performance of an oral dark borosilicate contrast media was evaluated on a clinical PCD-CT at different tube potentials and VMI energy levels. The CNR of DBCM against iodine image contrast was substantially higher than the CNR of water against iodine. This finding may indicate that hyperenhancing small bowel pathologies such as inflammation and neoplasia may be more conspicuous using DBCM with low-energy threshold images at higher kV or VMIs using an optimal keV on PCD-CT from 50 to 70 keV. Further study is needed to determine if this increased image contrast can be translated into improved radiologist performance for specific diagnostic tasks in small bowel imaging.

Supplementary Material

Refer to Web version on PubMed Central for supplementary material.

Acknowledgements

Research reported in this publication was supported by the National Institute of Diabetes and Digestive and Kidney Diseases of the National Institutes of Health under Award Number R44DK103495. The content is solely the responsibility of the authors and does not necessarily represent the official views of the National Institutes of Health. The authors thank Kevin Kimlinger for assistance in manuscript editing, preparation, and submission.

Conflicts of Interest

Y. Sun is an employee and shareholder of Nextrast, Dr. Yeh is a shareholder of Nextrast, consultant for General Electric Healthcare, and receives patent royalties from UCSF. Dark Borosilicate Contrast Material (DBCM) remains experimental and is not FDA approved for clinical use. Drs. McCollough and Fletcher receive grant support

from Siemens. No other potential conflicts of interest were declared. Some of the information contained in the manuscript was presented at the Radiological Society of North America 2022 annual meeting, Chicago, IL.

Reference

1. Winklhofer S, Lin W-C, Wang ZJ, Behr SC, Westphalen AC, Yeh BM. Comparison of Positive Oral Contrast Agents for Abdominopelvic CT. American Journal of Roentgenology. 2019;212(5):1037–1043. [PubMed: 30835523]
2. Carney BW, Khatri G, Shenoy-Bhangle AS. The role of imaging in gastrointestinal bleed. Cardiovascular Diagnosis and Therapy. 2019.S88–S96. [PubMed: 31559156]
3. Murphy B, Winter DC, Kavanagh DO. Small Bowel Gastrointestinal Bleeding Diagnosis and Management—A Narrative Review. Frontiers in Surgery. 2019;6. [PubMed: 30949483]
4. Bruining DH, Zimmermann EM, Loftus EV, et al. Consensus Recommendations for Evaluation, Interpretation, and Utilization of Computed Tomography and Magnetic Resonance Enterography in Patients With Small Bowel Crohn's Disease. Gastroenterology. 2018;154(4):1172–1194. [PubMed: 29329905]
5. Gerson LB, Fidler JL, Cave DR, Leighton JA. ACG Clinical Guideline: Diagnosis and Management of Small Bowel Bleeding. Official journal of the American College of Gastroenterology | ACG. 2015;110(9):1265–1287.
6. Huprich JE, Fletcher JG, Fidler JL, et al. Prospective Blinded Comparison of Wireless Capsule Endoscopy and Multiphase CT Enterography in Obscure Gastrointestinal Bleeding. Radiology. 2011;260(3):744–751. [PubMed: 21642417]
7. Kammerer S, Höink AJ, Wessling J, et al. Abdominal and pelvic CT: is positive enteric contrast still necessary? Results of a retrospective observational study. European Radiology. 2015;25(3):669–678. [PubMed: 25316055]
8. Panagiotopoulou PB, Courcoutsakis N, Tentes A, Prassopoulos P. CT imaging of peritoneal carcinomatosis with surgical correlation: a pictorial review. Insights into Imaging. 2021;12(1):168. [PubMed: 34767065]
9. Leander P, Adnerhill I, Böök O, Casal-Dujat L, Stathis G, Fork T. A novel food-based foam as oral contrast agent with negative Hounsfield units for demarcation of small bowel loops on abdominal CT: tolerability and bowel distension in 25 volunteers. Acta Radiologica. 2021;62(12):1559–1566. [PubMed: 33251810]
10. Ramsay DW, Markham DH, Morgan B, Rodgers PM, Liddicoat AJ. The Use of Dilute Calogen®as a Fat Density Oral Contrast Medium in Upper Abdominal Computed Tomography, Compared with the Use of Water and Positive Oral Contrast Media. Clinical Radiology. 2001;56(8):670–673. [PubMed: 11467870]
11. Obmann MM, Sun Y, An C, Ohliger MA, Wang ZJ, Yeh BM. Bowel Peristalsis Artifact on Dual-Energy CT: In Vitro Study on the Influence of Different Dual-Energy CT Platforms and Enteric Contrast Agents. American Journal of Roentgenology. 2021;218(2):290–299. [PubMed: 34406059]
12. Flohr T, Petersilka M, Henning A, Ulzheimer S, Ferda J, Schmidt B. Photon-counting CT review. Physica Medica. 2020;79:126–136. [PubMed: 33249223]
13. Hsieh SS, Leng S, Rajendran K, Tao S, McCollough CH. Photon Counting CT: Clinical Applications and Future Developments. IEEE Transactions on Radiation and Plasma Medical Sciences. 2021;5(4):441–452. [PubMed: 34485784]
14. Leng S, Bruesewitz M, Tao S, et al. Photon-counting Detector CT: System Design and Clinical Applications of an Emerging Technology. RadioGraphics. 2019;39(3):729–743. [PubMed: 31059394]
15. Rajendran K, Petersilka M, Henning A, et al. First Clinical Photon-counting Detector CT System: Technical Evaluation. Radiology. 2022;303(1):130–138. [PubMed: 34904876]
16. Rajendran K, Voss BA, Zhou W, et al. Dose Reduction for Sinus and Temporal Bone Imaging Using Photon-Counting Detector CT With an Additional Tin Filter. Investigative Radiology. 2020;55(2):91–100. [PubMed: 31770297]

17. Higashigaito K, Euler A, Eberhard M, Flohr TG, Schmidt B, Alkadhi H. Contrast-Enhanced Abdominal CT with Clinical Photon-Counting Detector CT: Assessment of Image Quality and Comparison with Energy-Integrating Detector CT. Academic Radiology. 2022;29(5):689–697. [PubMed: 34389259]

18. Jungblut L, Kronenberg D, Mergen V, et al. Impact of Contrast Enhancement and Virtual Monoenergetic Image Energy Levels on Emphysema Quantification: Experience With Photon-Counting Detector Computed Tomography. Investigative Radiology. 2022;57(6):359–365. [PubMed: 35066533]

19. McNamara MM, Little MD, Alexander LF, Van Carroll L, Mark Beasley T, Morgan DE. Multireader evaluation of lesion conspicuity in small pancreatic adenocarcinomas: complimentary value of iodine material density and low keV simulated monoenergetic images using multiphasic rapid kVp-switching dual energy CT. Abdominal Imaging. 2015;40(5):1230–1240. [PubMed: 25331567]

20. Patel BN, Thomas JV, Lockhart ME, Berland LL, Morgan DE. Single-source dual-energy spectral multidetector CT of pancreatic adenocarcinoma: Optimization of energy level viewing significantly increases lesion contrast. Clinical Radiology. 2013;68(2):148–154. [PubMed: 22889459]

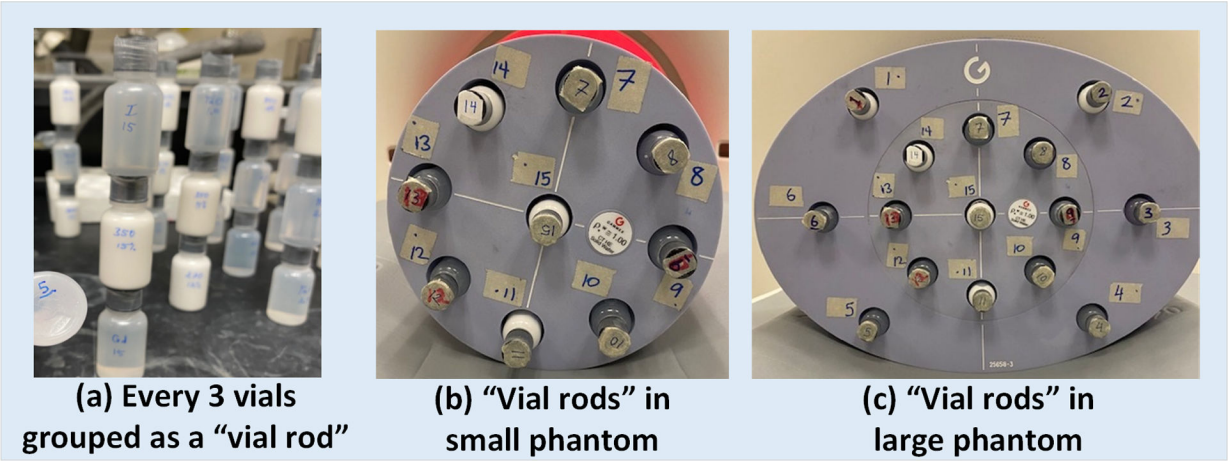

Figure 1.

(a) Vials containing various contrast materials were prepared and grouped in threes as a “vial rod”; these “vial rods” were labeled and inserted into the slots on the (b) small and (c) large phantoms.

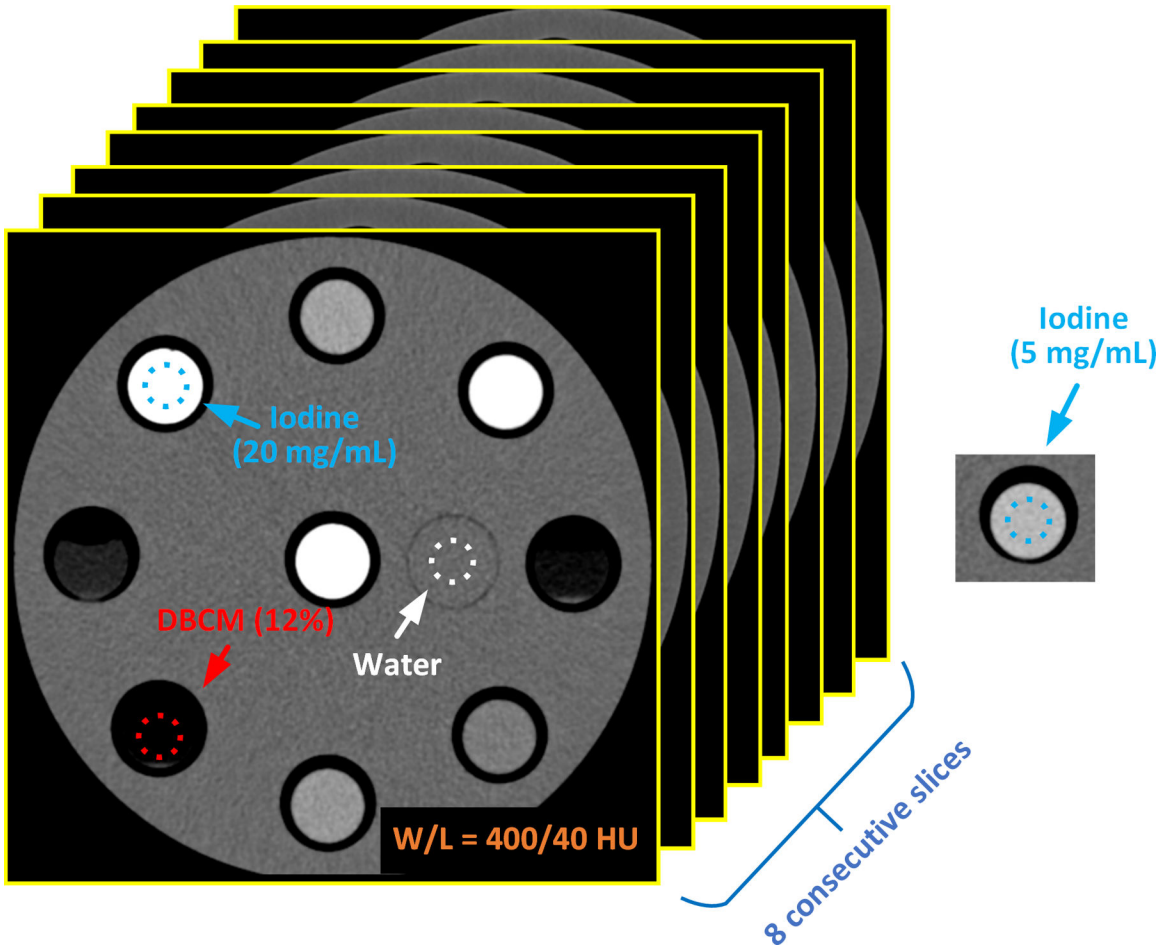

Figure 2.
Examples of ROI selections on iodine, DBCM, and solid-water; eight consecutive slices were involved in the measurements of CT number, noise, and contrast-to-noise ratio (CNR)

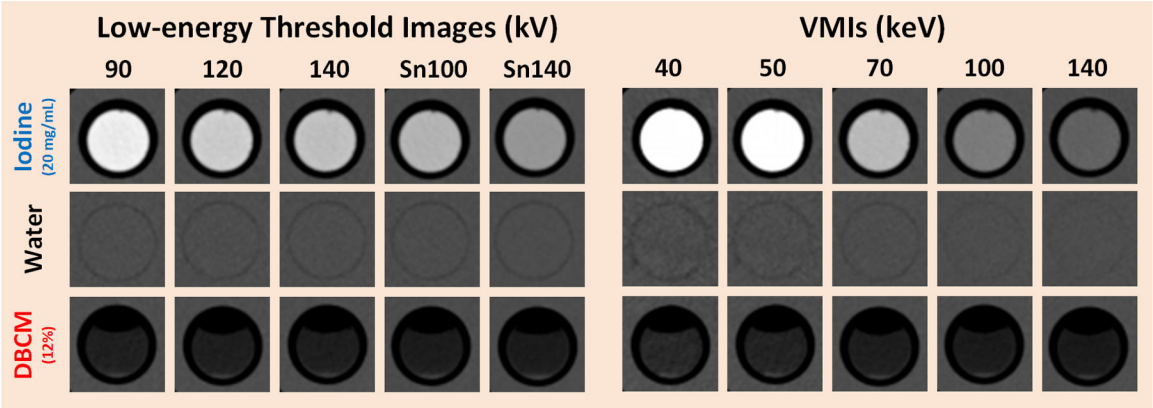

Figure 3.

Low-energy threshold photon-counting CT images acquired at five kV levels (left) and VMIs at 40, 50, 70, 100, and 140 keV (right) generated from the small phantom; iodine at 20 mg/mL (top), DBCM at 12% (bottom), and water (middle) are cropped and displayed for visual comparison. Note that the CT numbers for iodine contrast media vary substantially across tube potentials and VMI energy levels, compared to little change in CT number for water and DBCM. Some of the DBCM vials contain an air-DBCM fluid level.

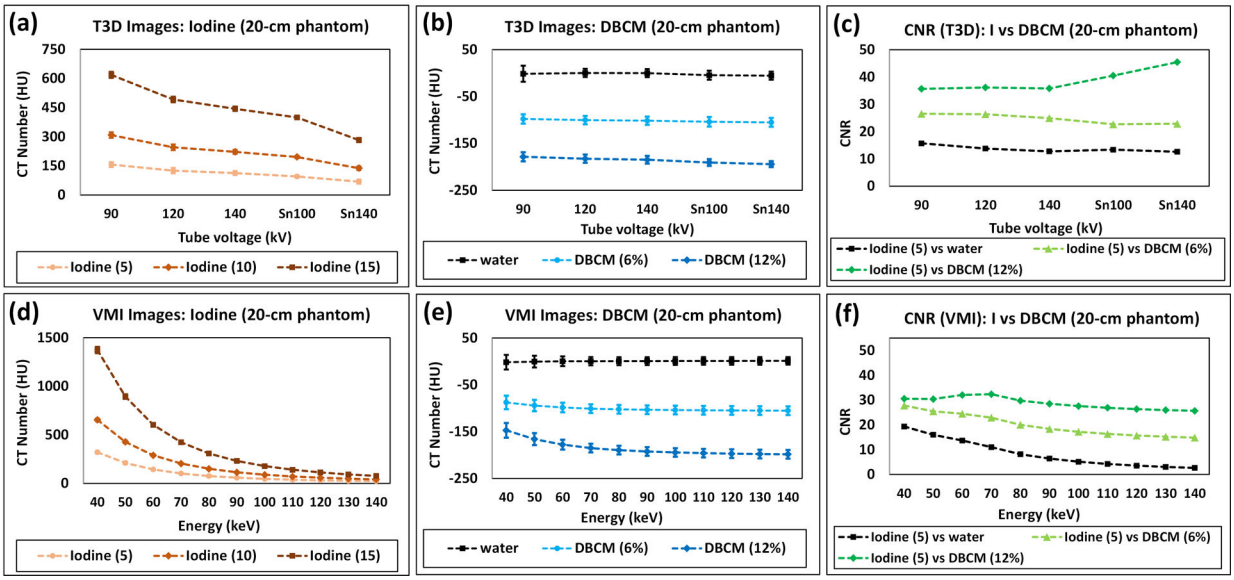

Figure 4.

Attenuation properties and CNR calculations for the small phantom: positive iodine image contrast measured using CT number on (a) low-energy threshold images and (d) VMIs; CT numbers measured for DBCM and water on (b) low-energy threshold images and (e) VMIs; CNR (Iodine against DBCM and Iodine against water) calculated on (c) low-energy threshold images and (f) VMIs.

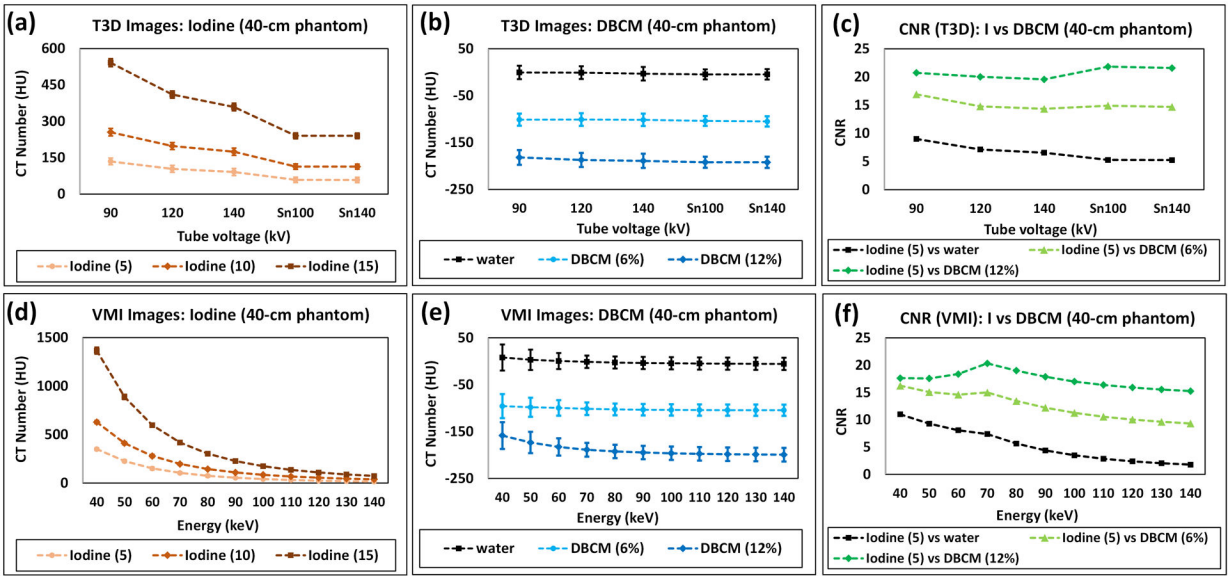

Figure 5.

Attenuation properties and CNR calculations for the large phantom: positive iodine image contrast measured using CT number on (a) low-energy threshold images and (d) VMIs; CT numbers measured for DBCM and water on (b) low-energy threshold images and (e) VMIs; CNR (Iodine against DBCM and Iodine against water) calculated on (c) low-energy threshold images and (f) VMIs.

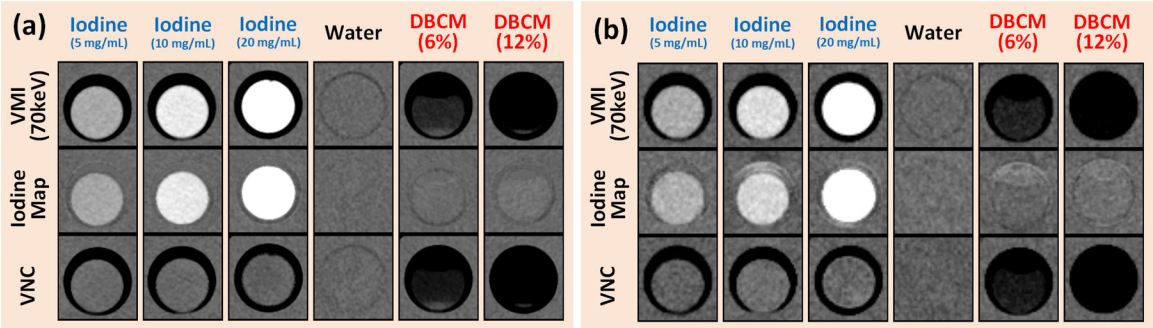

Figure 6.

VMI at 70 keV (top), iodine maps (middle), VNC (bottom) showing (left to right) iodine at 5, 10, and 20 mg/mL, water, DBCM-6%, and DBCM-12% for (a) 20 cm phantom and (b) 40 cm phantom. Note that all images were derived from a multi-energy scan at 120 kV.

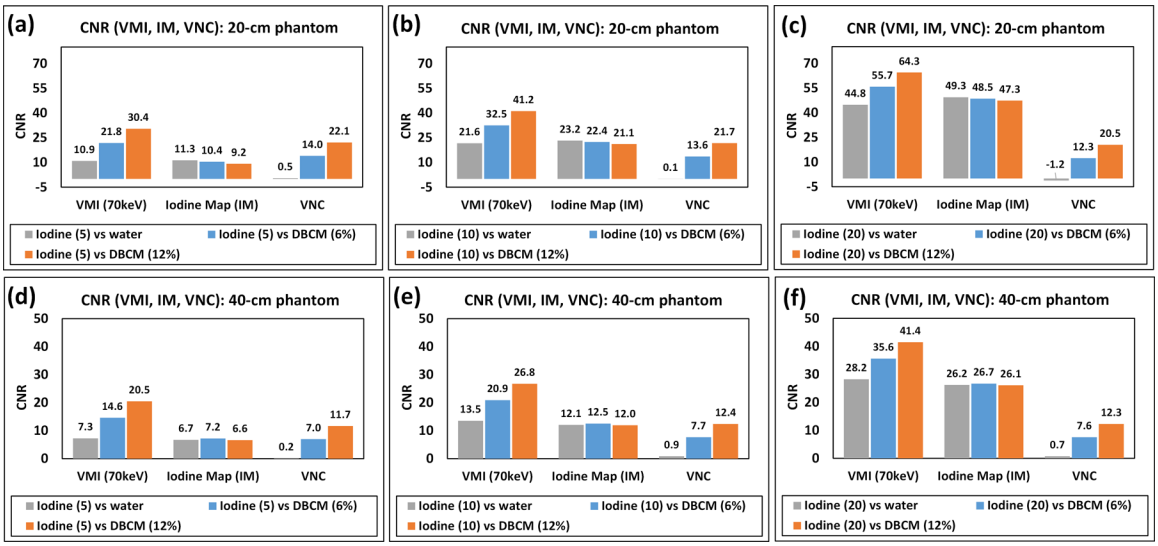

Figure 7.

CNR of iodine at (a,d) 5 mg/mL, (b,e) 10 mg/mL, and (c,f) 20 mg/mL again water or DBCM calculated on 70 keV VMI, iodine map (IM), and VNC for (a)–(c) 20-cm phantom, and (d)–(f) 40-cm phantom.

Table 1.

Data acquisition and image reconstruction parameters

Parameters		PCD-CT (NAEOTOM Alpha)
Scan	Automatic Exposure Control	CARE Dose 4D & CARE keV: Manual kV
	kV	90, 120, 140, Sn100, and Sn140
	CARE keV IQ level	180
	Collimation (mm)	144 × 0.4
	CTDIvol (mGy)	3.0 (small phantom) 12.0 (large phantom)
Reconstruction	Image type	Low-energy threshold (T3D) images (all kV levels)
		VMI: 40 to 130 keV at 90 kV 40 to 140 keV at 120 and 140 kV 60 to 140 keV at Sn100 and Sn140 kV (keV step: 10 keV) Iodine maps * Virtual noncontrast (VNC) *
	Slice-thickness/increment (mm)	2.0/2.0
	Kernel and QIR strength	Qr40 (QIR-2)

* Iodine maps and VNC images were reconstructed using multi-energy CT data obtained at a tube potential of 120 kV only, with the low threshold set at 20 keV, and a high energy threshold set at 65 keV.

Table 2.

Summary of CT number measurements on 70 keV VMI, iodine map, and VNC

Phantom Size	Spectral Recon Type	CT Number (HU) ± Noise					
		Iodine (5 mg/mL)	Iodine (10 mg/mL)	Iodine (15 mg/mL)	Water	DBCM-6%	DBCM-12%
20-cm	VMI (70 keV)	102.6±8.6	204.4±8.9	425.5±8.8	1.0±9.5	−102.9±8.5	−188.3±7.9
	Iodine Map	101.9±8.4	205.8±7.8	436.5±9.3	−0.1±9.7	7.0±8.0	21.5±8.2
	VNC	1.1±9.3	−0.5±7.8	−13.3±10.2	0.1±10.3	−127.4±6.8	−208.7±8.0
40-cm	VMI (70 keV)	105.9±13.7	197.0±13.4	404.9±14.6	1.2±13.6	−106.0±12.3	−192.0±18.7
	Iodine Map	112.6±15.2	194.0±13.4	394.5±20.0	9.4±15.2	3.5±14.8	10.6±12.8
	VNC	−9.1±15.4	1.4±12.5	10.9±15.9	−11.7±15.4	−125.9±10.8	−203.2±12.1